Use of General Regression Neural Networks for Generating the GLASS Leaf Area Index Product From Time-Series MODIS Surface Reflectance

Zhiqiang Xiao, Shunlin Liang, *Senior Member, IEEE*, Jindi Wang, Ping Chen, Xuejun Yin, Liqiang Zhang, and Jinling Song

***Abstract*—Leaf area index (LAI) products at regional and global scales are being routinely generated from individual instrument data acquired at a specific time. As a result of cloud contamination and other factors, these LAI products are spatially and temporally discontinuous and are also inaccurate for some vegetation types in many areas. A better strategy is to use multi-temporal data. In this paper, a method was developed to estimate LAI from time-series remote sensing data using general regression neural networks (GRNNs). A database was generated from Moderate-Resolution Imaging Spectroradiometer (MODIS) and CYCLOPES LAI products as well as MODIS reflectance products of the BELMANIP sites during the period from 2001–2003. The effective CYCLOPES LAI was first converted to true LAI, which was then combined with the MODIS LAI according to their uncertainties determined from the ground-measured true LAI. The MODIS reflectance was reprocessed to remove remaining effects. GRNNs were then trained over the fused LAI and reprocessed MODIS reflectance for each biome type to retrieve LAI from time-series remote sensing data. The reprocessed MODIS reflectance data from an entire year were inputted into the GRNNs to estimate the 1-year LAI profiles. Extensive validations for all biome types were carried out, and it was demonstrated that the method is able to estimate temporally continuous LAI profiles with much improved accuracy compared with that of the current MODIS and CYCLOPES LAI products. This new method is being used to produce the Global Land Surface Satellite LAI products in China.**

***Index Terms*—General regression neural networks (GRNNs), leaf area index (LAI), Moderate-Resolution Imaging Spectroradiometer (MODIS), retrieval, time series.**

I. Introduction

LEAF area index (LAI), defined as one half of the total green leaf area per unit of horizontal ground surface area [1], is often called true LAI. The true LAI multiplied by the clumping index is termed effective LAI [2]. LAI is an important biophysical variable that is widely applied for crop growth monitoring, yield estimation, land surface process simulation, and global change studies. The estimation of LAI from remote sensing data is the only feasible way to generate LAI products at the regional and, in particular, global scale.

There are currently two main types of methods for retrieving LAI from satellite data: empirical methods and physical methods. The empirical methods are based on statistical relationships between LAI and spectral vegetation indexes, which are calibrated for distinct vegetation types using field measurements of LAI and reflectance data recorded by a remote sensor or simulations from canopy radiation models [3]. Sellers *et al.* [4] retrieved LAI from Fourier Adjusted, Solar zenith angle correction, Interpolation, and Reconstruction of Normalized Difference Vegetation Index (NDVI) data using empirical relationships derived from available field surveys. Based on radiative transfer simulations and field surveys, Myneni *et al.* [5] derived biome-specific LAI–NDVI relationships and generated the corresponding LAI data sets from Pathfinder AVHRR Land and Global Inventory Modeling and Mapping Studies NDVI data. Chen *et al.* [6] derived Canada-wide time series of LAI from AVHRR and SPOT-Vegetation data using the land-cover-specific SR–LAI and RSR–LAI relationships. These empirical methods are computationally efficient in operating with a large amount of data, but they do not exploit the full spectral-directional information conveyed by the radiometric signal [7].

The physical methods are based on the inversion of canopy radiative transfer models through iterative minimization of a cost function [8], [9] or other methods. Because the model-inversion methods can be adjusted for a wide range of situations [10], radiative transfer models are increasingly used in the inverse mode to estimate LAI from remotely sensed data. However, inversion techniques based on iterative minimization of a cost function require hundreds of runs of the canopy radiative transfer model for each pixel; therefore, they are computationally too demanding [10]. For operational applications, look-up tables (LUTs) and artificial neural networks (ANNs) are two popular inversion techniques that are based on a pre-computed reflectance database. The LUT methods consist of determining the distribution of pre-computed canopy realizations that minimize a given misfit function with respect to

Manuscript received January 30, 2012; revised August 31, 2012 and December 21, 2012; accepted December 28, 2012. Date of publication February 6, 2013; date of current version November 26, 2013. This work was supported in part by the Chinese project entitled "Generation and Application of Global Products of Essential Land Variables" under Grant 2009AA122100 under the "State Program for High-Tech Research and Development (863 program)," the Chinese 973 Program under Grant 2013CB733403, the NASA Terrestrial Ecology Program, the National Natural Science Foundation of China under Grants 41171264 and 40871163, and the European Commission (Call FP7-ENV-2007-1 Grant 212921) as part of the CEOP-AEGIS project.

Z. Xiao, J. Wang, P. Chen, X. Yin, L. Zhang, and J. Song are with the State Key Laboratory of Remote Sensing Science, School of Geography, Beijing Normal University, Beijing 100875, China (e-mail: zhqxiao@bnu.edu.cn).

S. Liang is with the Department of Geography, University of Maryland, College Park, MD 20742, USA (e-mail: sliang@geog.umd.edu).

Color versions of one or more of the figures in this paper are available online at http://ieeexplore.ieee.org.

Digital Object Identifier 10.1109/TGRS.2013.2237780

the observations. Based on the radiative-transfer-model-based LUT, Myneni *et al.* [11] developed an operational algorithm to retrieve LAI from Moderate-Resolution Imaging Spectroradiometer (MODIS) data, and global LAI products have been generated from Terra and Aqua MODIS data with this algorithm since 2000.

ANNs are well known for their good performance in classification and function approximation. They are very efficient from a computational point of view, which is particularly important for operational applications with a long time series of global data. Currently, neural networks are increasingly being used for the estimation of LAI from remotely sensed data [3], [12]. Fang and Liang [13] demonstrated a neural network algorithm for retrieving LAI from the Landsat-7 Enhanced Thematic Mapper Plus surface reflectance and TOA radiance. Bacour *et al.* [8] developed an operational algorithm based on neural networks to estimate LAI, fAPAR, fCover, and LAI×Cab from MERIS top-of-canopy observations. Baret *et al.* [14] developed an algorithm for generating LAI, fAPAR, and fCover estimates from VEGETATION observations based on training neural networks with SAIL+PROSPECT radiative transfer model simulations for each biophysical variable. Verger *et al.* [15] evaluated the performance of a neural network approach to estimating LAI from CYCLOPES and MODIS nadir-normalized reflectance and LAI products. The neural networks were trained with the LAI products from one sensor and the reflectance from another.

Nevertheless, these methods use only remote sensing data acquired at a specific time to retrieve LAI. As a result of this use of limited information in the inversion process, the LAI products generated using these methods at regional or global scales are not spatially and temporally continuous [16] and are inaccurate for some vegetation types [17], [18]. An obvious solution to these problems is to use as much remotely sensed information as possible, both spatially and temporally. Xiao *et al.* [19] developed an algorithm using spatial contextual information to estimate canopy biophysical variables from high-resolution remote sensing images. Xiao *et al.* [8] developed a temporally integrated inversion method to estimate LAI from time-series MODIS reflectance data by coupling a double logistic LAI temporal profile model with a radiative transfer model. A similar method has been applied to retrieve LAI by combining MODIS albedo data with a dynamic leaf model [20]. Xiao *et al.* [21] developed a real-time inversion method to estimate LAI from MODIS time-series reflectance data using the ensemble Kalman filter. The LAI values are updated recursively by combining predictions from the dynamic model and MODIS reflectance data, and LAI can be predicted using the dynamic model in the absence of observations. All of these studies have demonstrated the capability of biophysical parameter retrieval supplied by time-series remote sensing observations.

The objective of this paper is to develop an operational method of estimating high-quality LAI with spatial completion and temporal continuity. To fully exploit the potential of multi-temporal remote sensing data and to take advantage of the several LAI products available, the reprocessed time-series MODIS reflectance were inputted into general regression neural networks (GRNNs) when trained with the fused time-series LAI from MODIS and CYCLOPES LAI products and the reprocessed MODIS reflectance of the BELMANIP sites during the period from 2001–2003. The retrieved LAI values were compared to the original CYCLOPES and MODIS LAI products and were also validated by ground LAI measurements.

The organization of this paper is as follows. Section II describes the experimental data, which include MODIS and CYCLOPES products and field LAI. Several details regarding the implementation of the algorithm, including expositions of the conversion from effective to true LAI and of the GRNNs used for LAI retrieval, are described in Section III. Comparisons of the LAI retrieved from time-series MODIS surface reflectance data by the GRNNs with the original MODIS and CYCLOPES LAI products and ground measurements are presented in Section IV. The paper concludes in Section V with a summary of the results.

II. Data

A. MODIS Products

MODIS reflectance (MOD09A1), LAI (MOD15A2), and land cover (MOD12Q1, layer 3) products are used in this study. All products, in a sinusoidal projection system, are from the latest version (Collection 5). These products were downloaded from http://wist.echo.nasa.gov/.

The MOD09A1 product provides the surface reflectance for each of the MODIS land spectral bands. The spatial resolution is 500 m, and the temporal sampling period is 8 days. We tested our methods for LAI estimation with red and near-infrared (NIR) reflectance time series.

The MODIS LAI has been produced since the year 2000 at a 1-km spatial resolution and an 8-day time step. The MODIS LAI retrieval algorithm includes a main algorithm and a backup algorithm. The main algorithm is based on LUTs simulated from a 3-D radiative transfer model for eight main biome classes. The MODIS red and NIR atmospherically corrected reflectances and the corresponding illumination-view geometries are used as inputs to the LUTs. The algorithm output is the mean LAI from all possible solutions within a specific level of input satellite data and model uncertainties. When the main algorithm fails, the backup algorithm is used to estimate LAI from biome-specific LAI–NDVI relationships [22].

In LAI retrieval algorithms, the manner to represented canopy architecture is a source of uncertainties that affect the estimation of LAI from surface reflectances. The three-dimensional plant canopy architecture is often characterized using the foliage clumping index [23]. Clumping occurs at several different scales including plant, canopy, and landscape. At the plant scale, it corresponds to the spatial distribution of foliage elements along plant stems or trunks, branches, and shoots for trees. At the canopy scale, clumping depends on the spatial arrangement of plants within the canopy. The clumping effect at the landscape scale is related to the physical aggregation of plant stands [24]. The MODIS LAI retrieval algorithm accounts for vegetation clumping at the canopy and plant (shoot) scales through 3-D radiative transfer formulations. Since the clumping values at landscape scale is not gathered as a function of biomes, it is partly addressed via mechanisms based

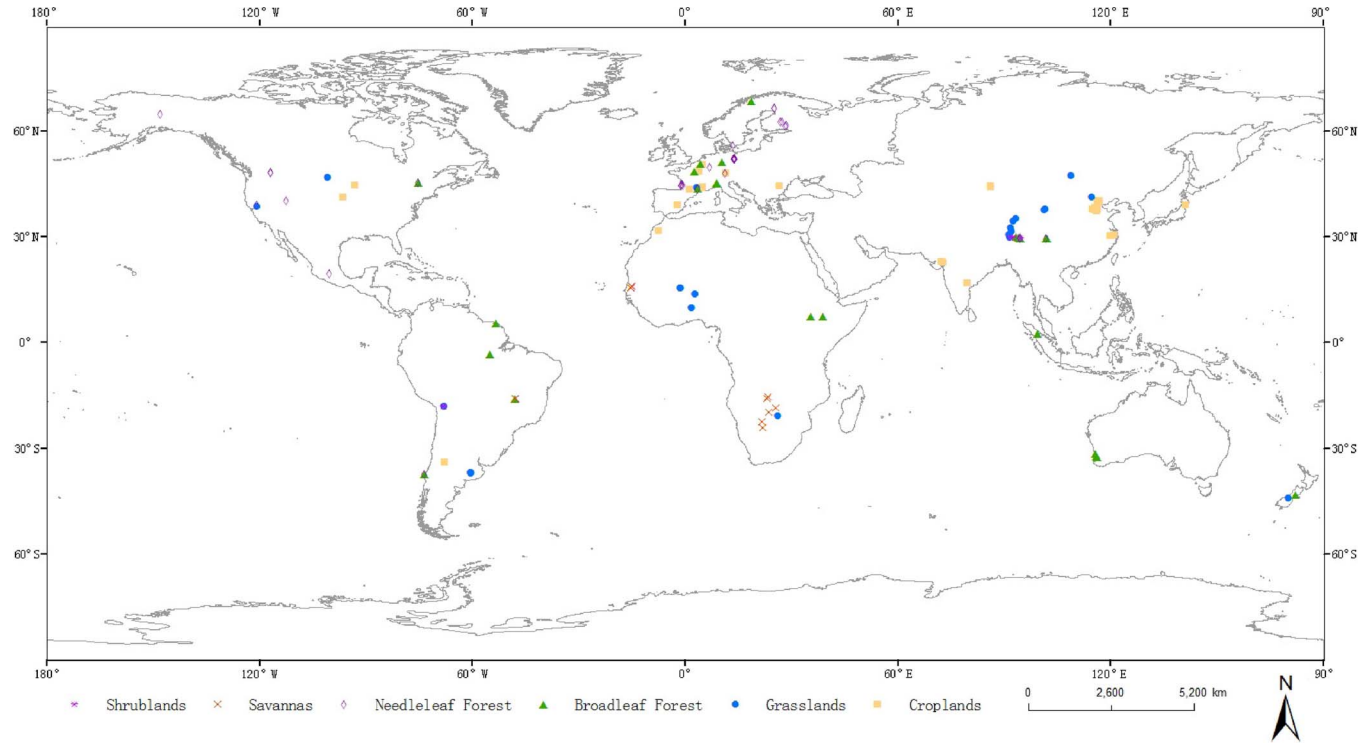

Fig. 1. Spatial distribution of ground-measured LAI.

on the radiative transfer theory of canopy spectral invariants in the MODIS LAI retrieval algorithm [22], [25]. Therefore, the MODIS LAI retrieval algorithm provides a true LAI.

The MODIS LAI retrieval algorithm uses the MODIS land cover type 3 (MOD12Q1) product [26] as *a priori* information with which to constrain the LAI space. The latest land cover yearly product (MCD12Q1) is at a 500-m spatial resolution and includes eight main biomes: grasses and cereal crops, shrubs, broadleaf crops, savannahs, evergreen broadleaf forests, deciduous broadleaf forests, evergreen needleleaf forests, and deciduous needleleaf forests. In addition, the product includes three non-biomes: unvegetated, urban, and water. In this paper, the MODIS land cover product is used for biome class distinction to train GRNNs for different biomes to estimate LAI from time-series MODIS surface reflectance data.

B. CYCLOPES LAI

The CYCLOPES LAI product, with a spatial resolution of 1/112° and a 10-day temporal sampling, is generated from SPOT/VEGETATION sensor data for the period 1999–2003 [14]. This product is projected in plate carrée.

The algorithm used to estimate LAI is based on training neural networks with PROSPECT+SAIL radiative transfer model simulations [14]. A nadir view of top-of-canopy reflectance in the red, NIR, and middle-infrared bands from VEGETATION sensors are the inputs to the neural networks, along with the sun zenith angle. However, the SAIL model has intrinsic limitations in its capacity to simulate heterogeneous canopies. Clumping at the plant and canopy scale is not represented in the CYCLOPES algorithm. Landscape clumping is partially taken into account by considering mixed pixels as a fraction of pure vegetation and pure bare soil when simulating the VEGETATION surface reflectance at the pixel level with the SAIL model. Thus, the CYCLOPES LAI retrieval algorithm provides an effective LAI.

Because the CYCLOPES and MODIS products use different projection systems, CYCLOPES products were reprojected into the MODIS projection system using the General Cartographic Transformation Package map projections library [27], and they were resampled to exhibit a 1-km spatial resolution using a bilinear interpolation technique.

C. Field LAI

In general, the uncertainties of moderate-resolution satellite products are assessed by analytical comparisons with field measurements, which are presumed to represent the target values [28]. There are many methods of collecting field LAI measurements. Generally, these measurement methods can be grouped into two categories: direct measurement and indirect measurement. The direct measurement methods obtain true LAI by using destructive samplings. The indirect measurement methods are based on an analysis of light transmittance through the canopy. Popular indirect optical methods include the LICOR LAI-2000, digital hemispherical photography (DHP), and Tracing Radiation and Architecture of Canopies (TRAC). These methods generally provide an effective LAI because they do not take foliage clumping into account, but the TRAC can provide a true LAI.

For this study, we collected worldwide LAI ground measurements from a total of 177 sites with different biome types.

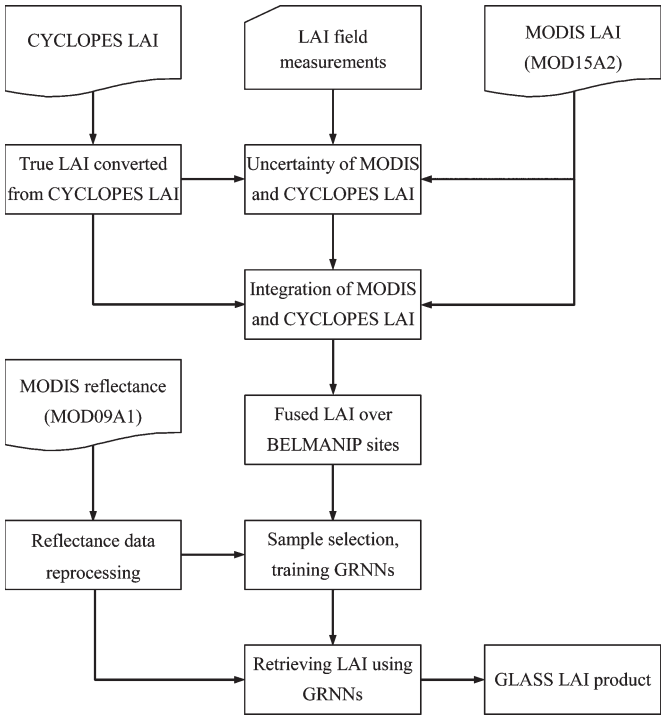

Fig. 2. Flow chart of LAI retrieval using general regression neural networks.

Cropland is the biome type with the largest number of sites (64), while the shrub and savannah biomes have relatively small numbers of sites (6 and 13, respectively). The spatial distribution of these ground-measured LAI is shown in Fig. 1. Most of the field LAI data were obtained from several existing networks (e.g., VALERI, BigFoot, and FluxNet) and published papers, while the others were obtained from the spectrum knowledge database of typical land surface objects [29]. These data were obtained with either direct measurement methods, such as destructive sampling, or indirect optical methods, such as the LAI2000, DHP, or TRAC methods. Therefore, some of the field data reflect the true LAI, while others are the effective LAI. A total of 21 sites from VALERI provide true and effective LAI simultaneously. The effective and true LAI at these sites are derived from the description of the gap fraction as a function of the view zenith angle. The effective LAI does not take the clumping effect into account, and the true LAI is derived using the method proposed by Lang and Xiang [30].

III. Methodology

The retrieval method proposed in this study employs GRNNs to retrieve LAI from time-series MODIS reflectance data. Different from the existing neural network methods that use only remote sensing data acquired at a specific time to retrieve LAI, GRNNs used in this study are trained with the fused time-series LAI from MODIS and CYCLOPES LAI products and the reprocessed MODIS reflectance. The reprocessed time-series MODIS reflectance were inputted into the GRNNs to estimate LAI profiles. A flow chart outlining this method is shown in Fig. 2.

A database was generated from MODIS and CYCLOPES LAI products and MODIS reflectance products of the BELMANIP sites during the period from 2001–2003. The effective CYCLOPES LAI was first converted to the true LAI, which was then combined with the MODIS LAI according to the uncertainties of each as determined from the ground-measured true LAI. The MODIS reflectance was reprocessed to remove remaining effects of cloud contamination and other factors. GRNNs were then trained using the fused LAI and reprocessed MODIS reflectance for each biome type. To retrieve LAI from time-series remote sensing data, the reprocessed MODIS reflectance data from an entire year were input to estimate 1-year LAI profiles using the GRNNs. Detailed descriptions of the new algorithm are given in the following subsections.

A. Conversion From Effective to True LAI

The field LAI from different measurement methods may be either the effective or true LAI, depending on the manner in which each method treats foliage clumping. Furthermore, LAI retrieved from remote sensing data can also be identified as true or effective LAI, depending on the inversion algorithms used. Therefore, there is great need for the development of a conversion relationship between effective and true LAI to be employed when integrating multiple LAI products or when using ground-measured LAI for analysis and validation of remote sensing products.

Conversion of Ground-Measured Effective LAI: VALERI provide effective and true LAI values for a total of 21 sites. The effective and true LAI values at these sites were acquired using either hemispherical photographs or LAI-2000 measurements (w3.avignon.inra.fr/valeri/). These data sets were used to establish linear regression models for the relationship between effective and true LAI for different vegetation types. However, the ground measurements for some biome types were not sufficient to establish reliable regression equations. Taking into account the characteristics of vegetation canopy structure, the ground measurements for the grass and savannah biomes were combined to establish a regression equation. Similarly, the ground measurements for the evergreen broadleaf forest, deciduous broadleaf forest, and shrub biomes were also combined to establish a regression equation, as were the evergreen needleleaf forest and deciduous needleleaf forest biomes. Then, the ground-measured effective LAI values, as described in Section II-C, were converted to the true LAI values following the application of these linear regression models.

Conversion of Cyclopes LAI: Because of the surface heterogeneity, the regression models for the relationship between effective LAI and true LAI from the ground-measured LAI values are not suitable for direct conversion of CYCLOPES-resolution pixels. In this paper, we used the clumping index derived from satellite data to convert the effective CYCLOPES LAI to true LAI.

Chen [2] demonstrated that the effective LAI is determined as the product of the true LAI and the clumping index, as follows:

$$LAI_e = \Omega \times LAI_t \tag{1}$$

where LAI_e is the effective LAI, LAI_t is the true LAI, and Ω is the clumping index. If Ω is known, we can convert between the effective LAI and true LAI using formula (1).

Based on the linear relationship between the clumping index and the normalized difference between hotspot and darkspot (NDHD) indexes, Chen *et al.* [31] derived the first global clumping-index map using multi-angular POLDER 1 satellite data from ADEOS-1. Pisek *et al.* [32] expanded the global mapping of the clumping index by integrating new, complete, year-round observations from POLDER 3. The across-biome difference in the topographical effect was removed in the new global clumping-index map. The spatial resolution of the global clumping-index map is 6 km.

Global average of the clumping index values for different biome types were derived according to MODIS land cover product. For each land cover class, the pixels in the global clumping-index map are selected to calculate the global average if the pixels with a fraction of at least 85% are covered with a single MODIS land cover type. This being the case, the CYCLOPES LAI for different vegetation types can be converted to the true LAI using formula (1).

As a result of cloud, atmospheric and snow contamination, there are missing LAI data, and the CYCLOPES LAI profiles exhibit time-series fluctuations during the growing season. Savitzky-Golay filtering was used to smooth and gap fill the CYCLOPES LAI. The time series of true LAI converted from CYCLOPES LAI are relatively smooth, and the true LAI values are larger than the CYCLOPES LAI values, particularly during the growing season.

B. Fusion of LAI From MODIS and CYCLOPES

It has been demonstrated that integrated LAI products have a much higher accuracy than the individual products [33]. In this paper, we attempted to estimate the fusion LAI from a linear combination of the MODIS LAI and the true CYCLOPES LAI values as follows:

$$LAI_{\mathrm{mod}\,cyc} = w_{\mathrm{mod}}\, LAI_{\mathrm{mod}} + w_{cyc} LAI^{*}_{cyc} \qquad (2)$$

where $LAI_{\mathrm{mod}\,cyc}$ is a combined estimate of LAI, LAI_{mod} is the smoothed and gap-filled MODIS LAI resulting from multi-step Savitzky-Golay filtering procedure [21], LAI^{*}_{cyc} is the true LAI converted from the CYCLOPES LAI using the method described in Section III-A, and w_{mod} and w_{cyc} are the normalized weights for the MODIS LAI and the true CYCLOPES LAI, respectively, the sum of these weights being equal to one. Thus, we can obtain the fusion LAI using formula (2) if the weights are known.

The weights may vary spatially and temporally, depending on the uncertainties of different products. To determine the weights in the absence of high-resolution LAI maps, the ground-measured LAI data were compared to the MODIS LAI and true CYCLOPES LAI with the same land cover type in the surrounding 3×3 pixels according to MODIS land cover descriptions.

From the ground-measured LAI data described in Section II-C and the corresponding MODIS LAI values,

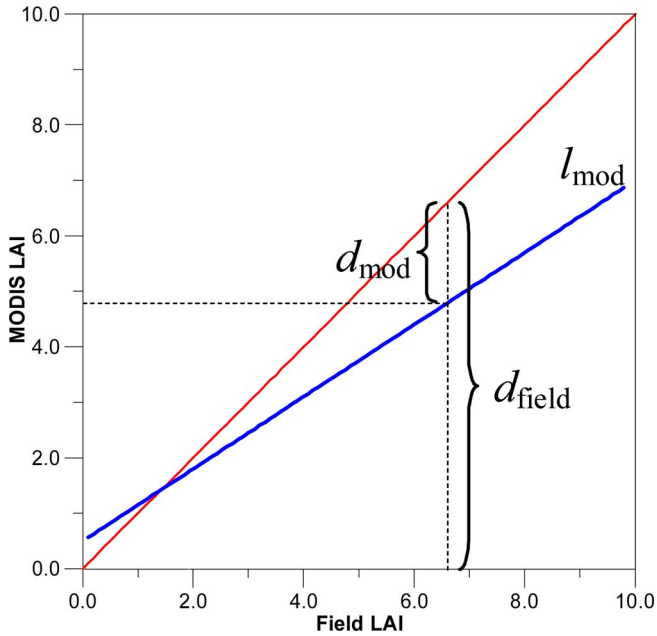

Fig. 3. Schematic diagram of the weight determination of the MODIS LAI.

a linear regression equation was determined for each biome type. The regression equation for a biome type is denoted by l_{mod} in Fig. 3. Let d denote the MODIS LAI value of a pixel at a particular time point; then, we can obtain the "field LAI" of this pixel at this time point by means of the regression equation. Let d_{field} denote the "field LAI," and let $d_{\mathrm{mod}} = |d - d_{\mathrm{field}}|$ denote the offset of the MODIS LAI value from the "field LAI." Then, $f_{\mathrm{mod}} = 1 - (d_{\mathrm{mod}}/d_{\mathrm{field}})$ reflects the relative accuracy of the MODIS LAI value of this pixel at this time point. The larger f_{mod} is, the more accurate the MODIS LAI value becomes, and vice versa. Similarly, the linear regression equation describing the relationship between the true CYCLOPES LAI, and the ground-measured LAI for each biome type was also found, from which we can obtain the relative accuracy of the true CYCLOPES LAI of this pixel at this time point. Let f_{cyc} denote the relative accuracy of the true CYCLOPES LAI. Then, the weights for the MODIS LAI and the true CYCLOPES LAI of this pixel at this time point are defined as follows:

$$w_{\mathrm{mod}} = f_{\mathrm{mod}}/(f_{\mathrm{mod}} + f_{cyc}) \qquad (3)$$

$$w_{cyc} = f_{cyc}/(f_{\mathrm{mod}} + f_{cyc}) \qquad (4)$$

It can be observed from formulas (3) and (4) that the weights of the MODIS LAI and the true CYCLOPES LAI are proportional to the relative accuracy of the MODIS LAI and the true CYCLOPES LAI values.

For each pixel, we can obtain the weights for MODIS LAI and true CYCLOPES LAI at any time point using formulas (3) and (4), and we can then obtain the combined estimates of LAI using formula (2). Fig. 4 shows the fused LAI time series for four different biome types. For convenient comparison, MODIS and CYCLOPES LAI and their corresponding weights are also shown in Fig. 4. Because the true CYCLOPES LAI is more consistent than the MODIS LAI with the ground-measured

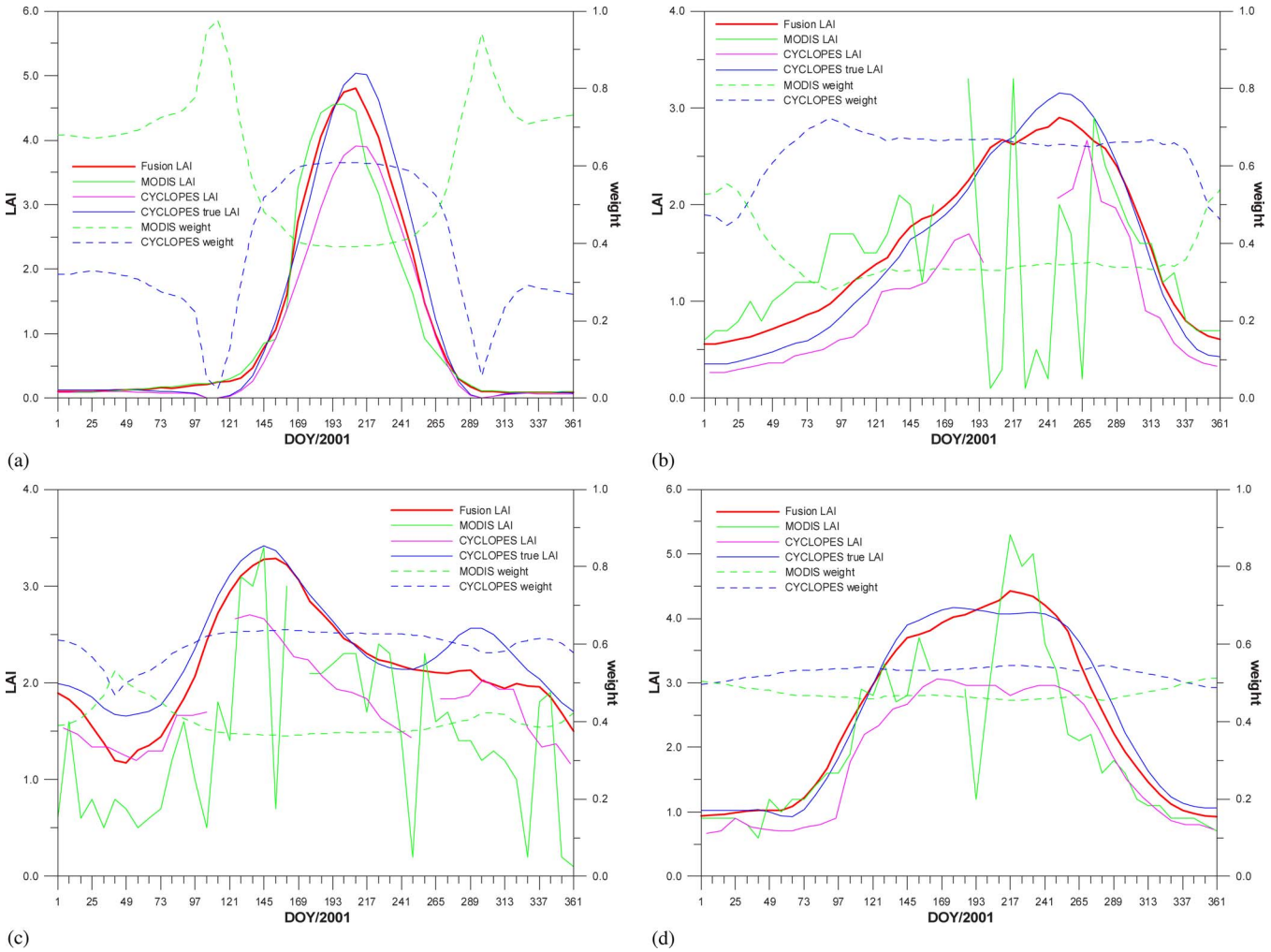

Fig. 4. Fused LAI time series from MODIS and CYCLOPES LAI values for different vegetation types: (a) crops, (b) grasses, (c) broadleaf forests, and (d) needleleaf forests.

LAI, the CYCLOPES weights are larger than the MODIS weights during the growing season.

C. Reprocessing of the MODIS Reflectance Products

The quality of MODIS reflectance products (MOD09A1) is affected by many factors, such as clouds, aerosols, water vapor, and ozone. Although many of these effects are removed through atmospheric corrections, the remaining effects can sometimes be very large and require further processing [34].

Much effort has been devoted to the development of reprocessing methods to remove residual atmospheric contamination from the reflectance. In this paper, the method developed by Tang *et al.* [35] was used for the MODIS reflectance reprocessing. Data contaminated by undetected and fallout clouds are identified in the MODIS reflectance data with MODIS snow and cloud mask data, the spectral characteristics of temporal and spatial continuity and correlation, and other auxiliary information. Then, the cloud-contaminated data are removed using temporal-spatial filtering algorithms, and the missing data are filled using an optimum interpolation algorithm to obtain continuous and smooth surface reflectance values. Detailed information regarding this reprocessing method for the MODIS reflectance is given by Tang *et al.* [35].

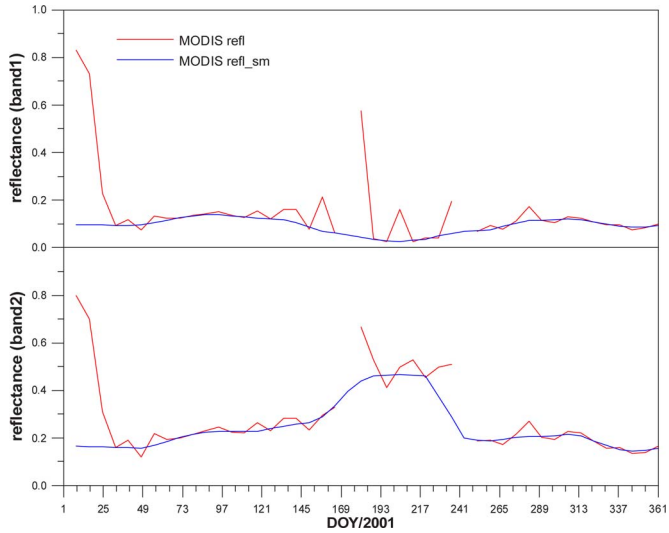

Fig. 5. Reprocessed reflectance and original MODIS reflectance in the R and NIR bands.

Fig. 5 shows the reprocessed reflectance in the red (R) and NIR bands at the Bondville site. It can be observed that the reprocessed reflectance is relatively smooth compared to the original MODIS reflectance.

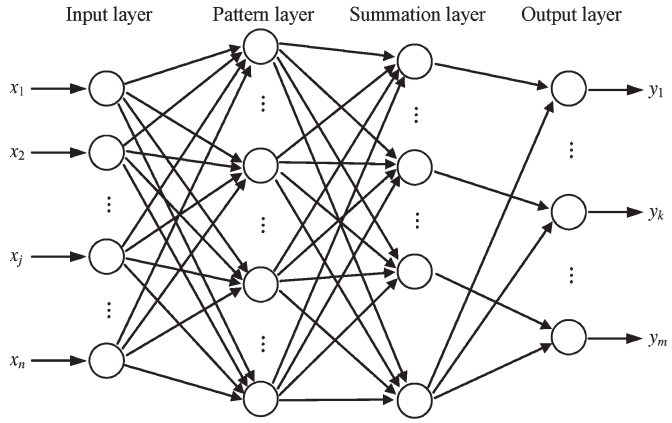

Fig. 6. GRNN with a multi-input-multi-output architecture.

D. LAI Inversion Using GRNNs

This study employed GRNNs to retrieve LAI products from the reprocessed time-series MODIS reflectance data. The GRNNs are trained using the fused time-series LAI from MODIS and CYCLOPES LAI products and the reprocessed MODIS reflectance values for each of the MODIS biome classes.

GRNNs*:* The GRNN, developed by Specht [36], is a generalization of radial basis function networks and probabilistic neural networks. The advantage of this type of neural network is that it can approximate the map inherent in any sample data set. In addition, GRNNs possess a special property, namely, these networks do not require iterative training. The functional estimate is computed directly from the training data. At present, GRNNs have been applied in a variety of fields, such as system identification, adaptive control, pattern recognition, and time-series prediction [37].

Fig. 6 shows a GRNN with a multi-input-multi-output architecture. It includes four layers, namely, the input layer, the pattern layer, the summation layer, and the output layer. The input layer provides all of the measurement variables to all of the neurons in the pattern layer; each neuron represents a training pattern, and the output of each neuron is a measure of the distance of the input from the stored patterns. The summation layer consists of two types of summation neurons: one type computes the summation of the weighted outputs of the pattern layer, where the weight for the ith neuron in the pattern layer is the target output value corresponding to the ith input pattern, and the other type calculates the unweighted outputs of the pattern neurons. Finally, the output layer performs the normalization step to compute the GRNN-predicted value of the output variable.

If the kernel function of the GRNN is Gaussian, the fundamental formulation of the GRNN is deduced as follows:

$$\mathbf{Y}'(\mathbf{X}) = \frac{\sum_{i=1}^{n} \mathbf{Y}^i \exp\left(-\frac{D_i^2}{2\sigma^2}\right)}{\sum_{i=1}^{n} \exp\left(-\frac{D_i^2}{2\sigma^2}\right)} \tag{5}$$

where $D_i^2 = (\mathbf{X} - \mathbf{X}^i)^T(\mathbf{X} - \mathbf{X}^i)$ represents the squared Euclidean distance between the input vector $\mathbf{X}$ and the ith training input vector $\mathbf{X}^i$, $\mathbf{Y}^i$ is the output vector corresponding to the vector $\mathbf{X}^i$, $\mathbf{Y}'(\mathbf{X})$ is the estimate corresponding to the vector $\mathbf{X}$, n is the number of samples, and σ is a smoothing parameter that controls the size of the receptive region. As σ becomes larger, the GRNN output approaches the mean of the training set outputs. As σ becomes smaller, the GRNN output approaches the output pattern of the training set. Formula (5) shows that the estimate $\mathbf{Y}'(\mathbf{X})$, given an input vector $\mathbf{X}$, is the weighted average of all the sample observations $\mathbf{Y}^i$, where the weight for each observation is proportional to the Euclidean distance between the vector $\mathbf{X}$ and the training input vector $\mathbf{X}^i$.

In this paper, the input vector $\mathbf{X}$ of the GRNNs used to retrieve LAI includes the reprocessed MODIS time-series reflectance values in the red (R) and NIR bands (for a 1-year period); that is, $\mathbf{X} = (R_1, R_2, \ldots, R_{46}, NIR_1, NIR_2, \ldots, NIR_{46})^T$ and contains 92 components. The output vector $\mathbf{Y}' = (LAI_1, LAI_2, \ldots, LAI_{46})^T$ is the corresponding time series of LAI for the year and contains 46 components. For each biome type, a GRNN was constructed according to the corresponding training database.

Generating the Training Database: To generate LAI products at the regional or global scale using the GRNNs, the training database should be globally representative of surface types and conditions. The BELMANIP network, which includes 402 sites, aims to provide a good sampling of biome types and conditions throughout the world [38]. For each BELMANIP site, a 3×3 subset of the MODIS and CYCLOPES LAI products and the MODIS reflectance products from the 2001– 2003 period was extracted. The MODIS LAI product represents a true LAI, while the CYCLOPES LAI product represents an effective LAI. After the CYCLOPES LAI was converted to the true LAI, the true CYCLOPES LAI and MODIS LAI were combined according to their uncertainties as determined from the ground-measured true LAI. The MODIS reflectance was reprocessed to remove remaining effects of cloud contamination and other factors. Then, the fused time-series LAI and the reprocessed MODIS reflectance values were used to train the GRNNs.

To achieve better performance and convergence, the values of the training inputs and outputs were normalized according to formula (6) before training the GRNNs

$$\mathbf{X}_{norm} = 2.0 \times (\mathbf{X} - \mathbf{X}_{\min})/(\mathbf{X}_{\max} - \mathbf{X}_{\min}) - 1 \tag{6}$$

where $\mathbf{X}_{\max}$ and $\mathbf{X}_{\min}$ are the maximum and minimum values, respectively, for variable $\mathbf{X}$, and $\mathbf{X}_{norm}$ is the normalized value corresponding to the training inputs or outputs $\mathbf{X}$.

Training of the GRNNs*:* In contrast to back-propagation neural networks, which are iteratively trained to determine the weights, the architecture and weights of GRNNs are determined when the input to the GRNN is given. The smoothing parameter σ is the only free parameter in the GRNN formulation. Therefore, the training of the GRNN is essentially the optimization of the smoothing parameter. The value of the smoothing parameter significantly affects the accuracy of the GRNN predictions. Thus, the magnitude of σ needs to be chosen carefully. Specht [36] suggested the use of the holdout method to find a suitable σ. For a particular value of σ, the holdout method consists of

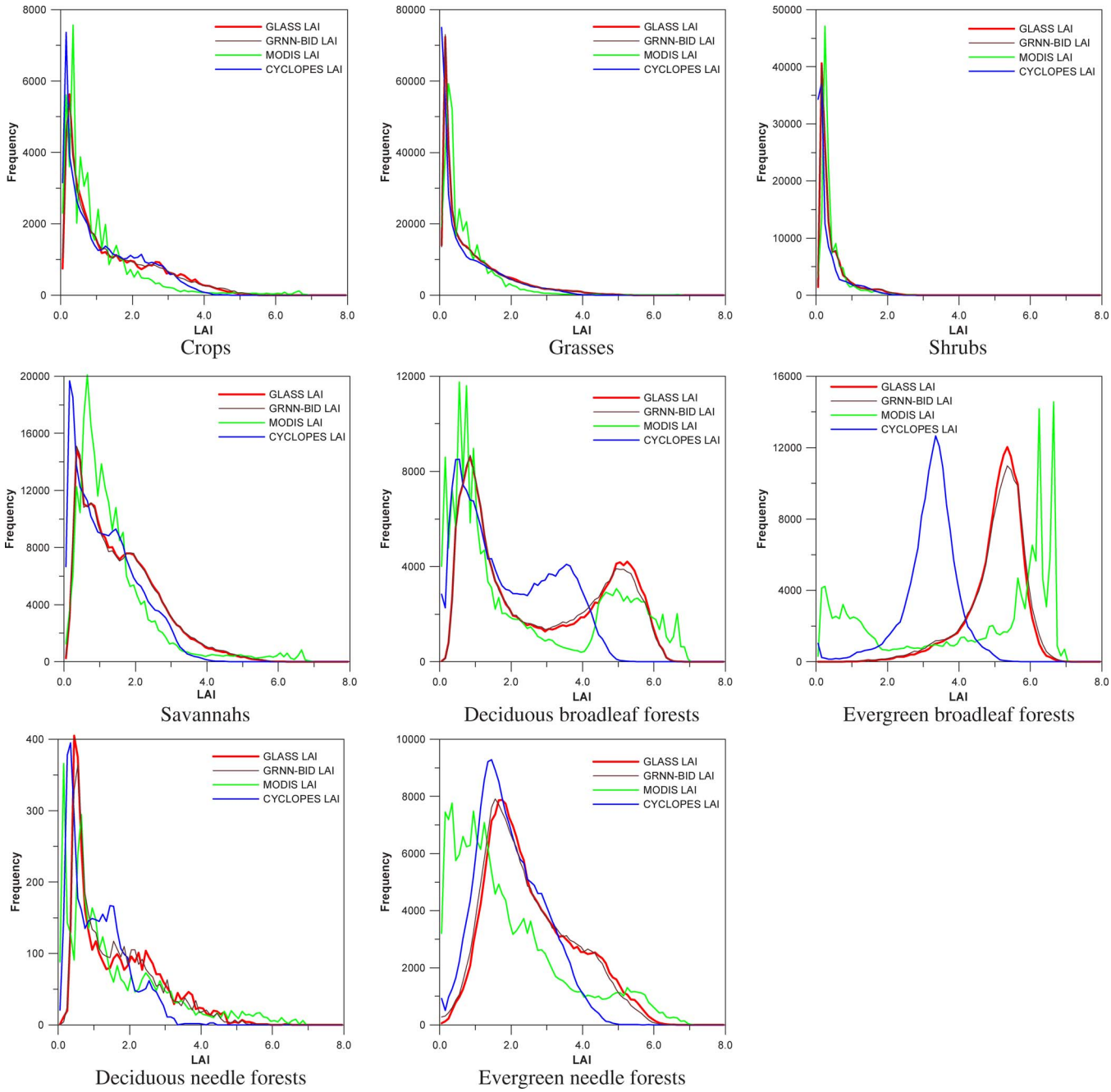

Fig. 7. Statistical distributions of GLASS and GRNN-BIN LAI estimates as well as MODIS and CYCLOPES LAI products from the BELMANIP sites corresponding to eight MODIS biome classes during the 2001–2003 period.

removing one sample from the training data set at a time and constructing a GRNN based on all of the other training samples. The GRNN is then used to estimate $\mathbf{Y}$ for the removed sample. By repeating this process for each sample and storing each estimate, the mean squared error between the actual sample values $\mathbf{Y}^i$ and the estimates can be evaluated. The value of σ giving the smallest error should be used in the final GRNN. In fact, for the GRNNs in this study, the learning period was completed when the minimum of the following cost function of the smoothing parameter was reached:

$$f(\sigma) = \frac{1}{n}\sum_{i=1}^{n}\left(\hat{\mathbf{Y}}_i(\mathbf{X}_i) - \mathbf{Y}_i\right)^2 \tag{7}$$

where $\hat{\mathbf{Y}}_i(\mathbf{X}_i)$ is the estimate corresponding to $\mathbf{X}_i$ using the GRNN trained over all of the training samples except the ith sample.

A variety of optimization methods are currently used to find the optimal smoothing parameter in formula (7). The most commonly used methods are the hill-climbing method and the conjugate gradient method. However, these are subject to becoming caught in local minima, and they can produce false minima. Hansen and Meservy [39] used the genetic algorithm to optimize the smoothing factor used to find the optimal regression surface of the GRNN for its global optimization. In this paper, the shuffled complex evolution method developed at the University of Arizona was used to obtain the optimal

smoothing parameter of the GRNN; this algorithm does not require the derivatives of the function, and it is not susceptible to being trapped by small pits and bumps on the function's surface [40]. It has also been extensively used in our recent studies [8], [41].

According to MODIS land cover, a dedicated GRNN was constructed for each biome type. Then, the trained GRNNs were used to retrieve LAI for the corresponding biome types from the reprocessed MODIS reflectance values. In addition, we also trained a GRNN using samples from all the biome types for comparison of the GRNNs per classes. The resultant trained GRNN can be used to retrieve LAI across all biomes. Therefore, it is biome independent.

IV. Results and Validation

In this section, the LAI retrieved using the GRNNs is compared with the original CYCLOPES and MODIS LAI products. Then, a comparison with ground measurements (direct validation) and a temporal analysis are presented.

A. Intercomparison

Histograms of LAI estimates using the biome-dependent GRNNs and the biome-independent GRNN (denoted by Global Land Surface Satellite (GLASS) LAI and GRNN-BID LAI, respectively) as well as the CYCLOPES and MODIS LAI products were analyzed from the BELMANIP sites of eight MODIS biome classes during the 2001–2003 period. The statistical distributions of these LAI products are shown in Fig. 7.

Histograms of the LAI values (Fig. 7) show that the distributions of the GLASS and GRNN-BID LAI values derived from the same reprocessed MODIS reflectance products are consistent with one another in each biome. For the crop, grass, shrub, savannah, and needle forest biome types, the histogram distributions of the GLASS and GRNN-BID LAI values are consistent with those of the CYCLOPES and MODIS LAI values.

For the evergreen broadleaf forest biome type, the GLASS and GRNN-BID LAI values exhibit a distribution with a narrow peak approximately 5.5, and the peak position (approximately 6.5) of the MODIS LAI frequency distribution is higher compared to the CYCLOPES, GLASS and GRNN-BID LAI values. This is partly due to the overestimation of MODIS LAI values associated with broadleaf forests [24]. In addition, CYCLOPES rarely produces LAI values larger than 4 for the broadleaf and needle forest biome types.

B. Direct Validation

For the assessment and validation of the moderate-resolution LAI products, ground "point" measurements are not suitable for making direct comparisons with moderate-resolution pixels due to the surface heterogeneity. Usually, high-resolution remotely sensed imagery is used to scale the ground LAI measurements up to moderate-resolution pixels. The high-resolution LAI maps generated from ground measurements are aggregated to produce a moderate resolution, and they are used to compare and evaluate moderate-resolution LAI products [42].

TABLE I
Characteristics of the Selected Sites

Site Name	Lat (°)	Lon (°)	Biome class	DOY	Year	True LAI
Alpilles	43.81	4.74	BC	201	2002	1.7
Konza	39.09	−96.57	GC	169	2001	2.9
				228	2001	2.6
Gilching	48.08	11.32	GC	189	2002	5.7
Tundra	71.27	−156.61	GC	227	2002	1.1
Sud-Ouest	43.51	1.24	GC	201	2002	2.3
Fundulea	44.41	26.58	GC	128	2001	3.0
				160	2002	1.6
Sevilleta	34.35	−106.69	GC	207	2002	0.1
				234	2002	0.3
				252	2002	0.4
				319	2002	0.3
				174	2003	0.1
				209	2003	0.0
				258	2003	0.1
				325	2003	0.1
Thompson	56.05	−98.16	NF	196	2001	1.6
NOBS-BOREAS	55.89	−98.48	NF	195	2001	3.5
				195	2002	3.2
Larose	45.38	−75.22	NF	231	2003	5.6
Nezer	44.57	−1.04	NF	111	2002	2.4
Counami	5.34	−53.24	BF	269	2001	4.9
				274	2002	4.4
Puechabon	43.72	3.65	BF	163	2001	2.9
Laprida	−36.99	−60.55	SN	317	2002	2.7
Larzac	43.94	3.12	SN	193	2002	0.9

BC = Broadleaf crops, GC = Grasses and cereal crops, NF = Needleleaf forests, BF = Broadleaf forests, SN = Savannahs.

Garrigues *et al.* [24] proposed a set of validation sites with high-resolution LAI maps between 2000 and 2004. To be consistent with the definition of LAI in this study, only the sites whose ground LAI measurements took into account the clumping effect were selected to compare and evaluate the GLASS and GRNN-BID LAI values with values derived from aggregated high-resolution LAI maps.

These selected sites include different biome classes, including broadleaf crops, grasses and cereal crops, needleleaf forests, broadleaf forests, and savannahs, according to MODIS land cover. The spatial coordinates of the validation sites, land cover, dates of ground measurement acquisitions, and mean LAI values from 3 km × 3 km site areas are provided in Table I.

The GLASS and GRNN-BID LAI estimates and the original MODIS and CYCLOPES LAI products were compared with direct ground measurements (Fig. 8). The GLASS and GRNN-BID LAI estimates as well as the CYCLOPES and MODIS LAI products were linearly interpolated to the acquisition date of the ground measurements.

A good agreement between the LAI estimates obtained from GRNN retrieval methods and from field measurements was observed for all biomes, but the GLASS LAI values [Fig. 8(a)] are in fairly better agreement with the ground measurements ($\mathrm{R2} = 0.87$ and $\mathrm{RMSE} = 0.64$) than the GRNN-BID LAI values [Fig. 8(b)] ($\mathrm{R2} = 0.84$ and $\mathrm{RMSE} = 0.69$). Compared with the MODIS LAI values [Fig. 8(c)], the GLASS and GRNN-BID LAI values are distributed more closely around the 1:1 line with the ground-based LAI values. Fig. 8(d) shows the scatter plot between the CYCLOPES LAI values and the field measurements. CYCLOPES does not reach high enough LAI values to properly characterize forests and underestimates the

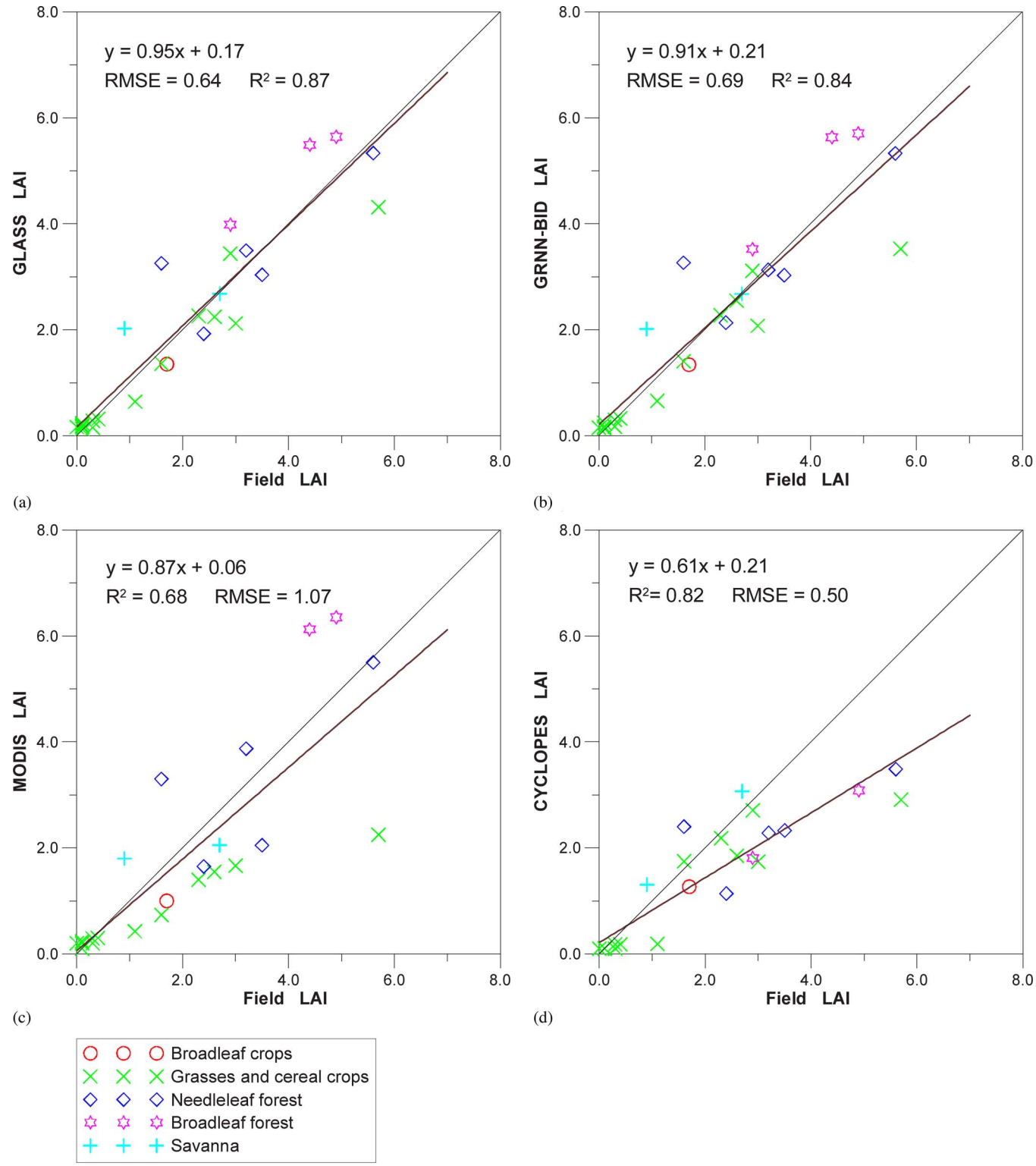

Fig. 8. Comparison of (a) GLASS, (b) GRNN-BID, (c) MODIS, and (d) CYCLOPES LAI values to ground measurements of LAI.

ground-based LAI values. This result is consistent with respect to the characteristics of the CYCLOPES algorithm, which does not include clumping at the shoot scale and thus should provide lower LAI estimates than the ground-based LAI values [24].

Overall, the GLASS and GRNN-BID LAI values are more accurate than the MODIS and CYCLOPES LAI estimates. However, we also note that more validation data with better representation of the global and seasonal vegetation variabilities are required to refine this result.

C. Temporal Profiles

The LAI temporal profiles of the central pixel for some sites in Table I are shown in Figs. 9–15. For a better evaluation of

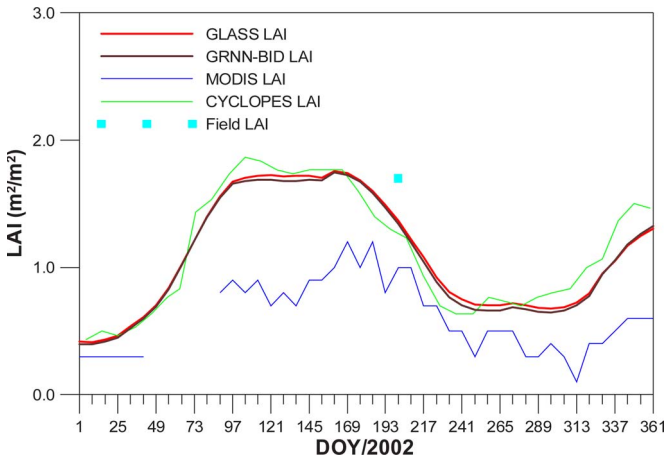

Fig. 9. Temporal profiles of GLASS, GRNN-BID, CYCLOPES, and MODIS LAI values of the Alpilles site for the year 2002.

the quality of the GLASS and GRNN-BID LAI values, the temporal profiles of CYCLOPES LAI values, MODIS LAI values, and ground measurements are also shown for each selected site.

Fig. 9 shows the temporal LAI trajectories over the Alpilles site for the year 2002. The biome type for this site is broadleaf crops, according to MODIS land cover. The GLASS, GRNN-BID, and CYCLOPES LAI values are in very good agreement for the entire year, while the MODIS LAI profile maintains lower LAI values compared to the GLASS, GRNN-BID, and CYCLOPES LAI profiles. Comparatively speaking, the GLASS and GRNN-BID LAI values are closer to the ground-based measurements than the MODIS and CYCLOPES LAI values. In Fig. 9, the MODIS data are so noisy, while all other LAI profiles are relatively smooth. Similar phenomena are also observed in Figs. 10–15. This is mainly due to high sensitivity of MODIS algorithm to surface reflectance uncertainties particularly at large LAI [43].

Figs. 10 and 11 show the temporal LAI trajectories over the BELMANIP sites with grass and cereal crop biome types according to MODIS land cover. In the Konza site, a good seasonality agreement is observed among the GLASS, GRNN-BID, CYCLOPES, and MODIS LAI values for the year 2001 [shown in Fig. 10(a)], although the MODIS LAI values for days 169 and 177 are missing. However, the GLASS and GRNN-BID LAI values are generally larger than the CYCLOPES and MODIS LAI estimates throughout the entire growing season, and the GRNN-BID LAI values are in better agreement with the few available ground measurements than the other LAI values. In Fig. 10(b), it can be observed that the GLASS LAI values are very close to the GRNN-BID LAI values and the ground measurements. However, large discrepancies can be observed between the GLASS and GRNN-BID LAI values and the MODIS and CYCLOPES LAI estimates. Before Julian day 135 in 2002, the GLASS and GRNN-BID LAI values were generally in very good agreement with the MODIS LAI estimates, while the CYCLOPES LAI magnitude was lower than that of all the other products. Conversely, the GLASS and GRNN-BID LAI values were generally in very good agreement with the CYCLOPES LAI estimates after Julian day 185 in 2002, while the MODIS LAI magnitude was lower than that of all the other products. Fig. 11 shows the LAI temporal

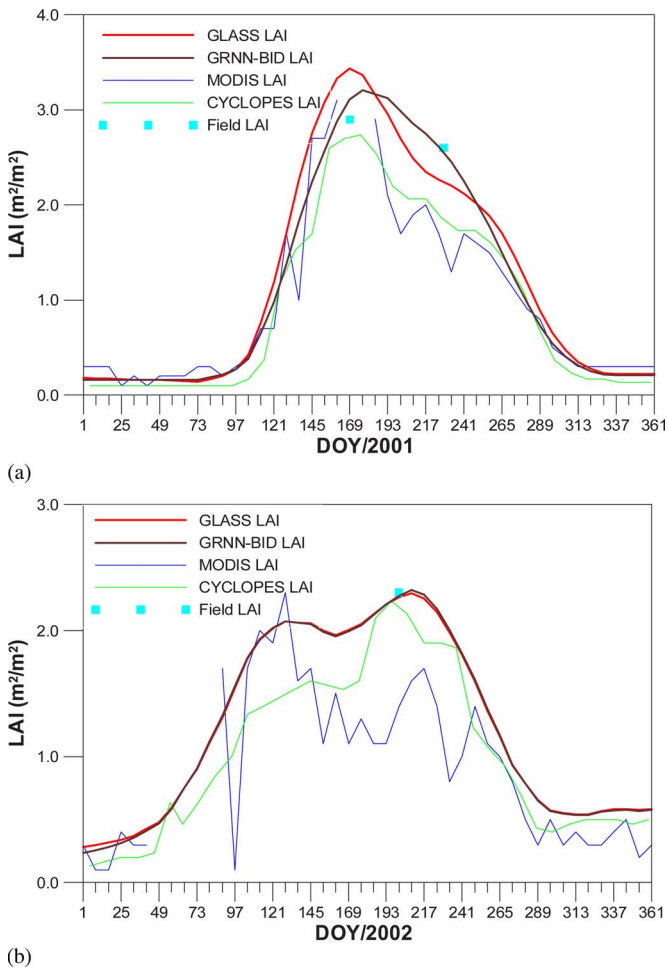

Fig. 10. Temporal profiles of GLASS, GRNN-BID, CYCLOPES, and MODIS LAI values for (a) the Konza site in 2001 and (b) the Sud-Ouest site in 2002.

profiles at the Fundulea site during the 2001–2002 period. The Fundulea site presents more interannual variability than other sites because its crops and cereals change from year to year. While a good seasonality agreement is achieved among the GLASS, GRNN-BID, CYCLOPES, and MODIS LAI values, they are all underestimates in comparison with the BELMANIP mean LAI data at this site in 2001.

Figs. 12 and 13 show the temporal LAI trajectories for the BELMANIP sites with the needleleaf forest biome type according to MODIS land cover. The MODIS LAI profile exhibits dramatic fluctuations for the NOBS-BOREAS site (shown in Fig. 12), and the CYCLOPES LAI values are missing for the winter because of large uncertainties in the reflectance data; in contrast, the temporal profiles of the GLASS and GRNN-BID LAI values during the 2001–2002 period are relatively smooth, and the accuracy of the GLASS and GRNN-BID LAI values is superior to those of the MODIS and CYCLOPES LAI values when compared to the BELMANIP mean LAI data at this site. In the Larose and Nezer sites (shown in Fig. 13), the LAI products generally depict similar temporal trajectories, although with differences in magnitude. The strongest agreement is achieved between the GLASS, GRNN-BID, and MODIS LAI values, aside from some fluctuations of the MODIS LAI values, while the CYCLOPES LAI values are significant

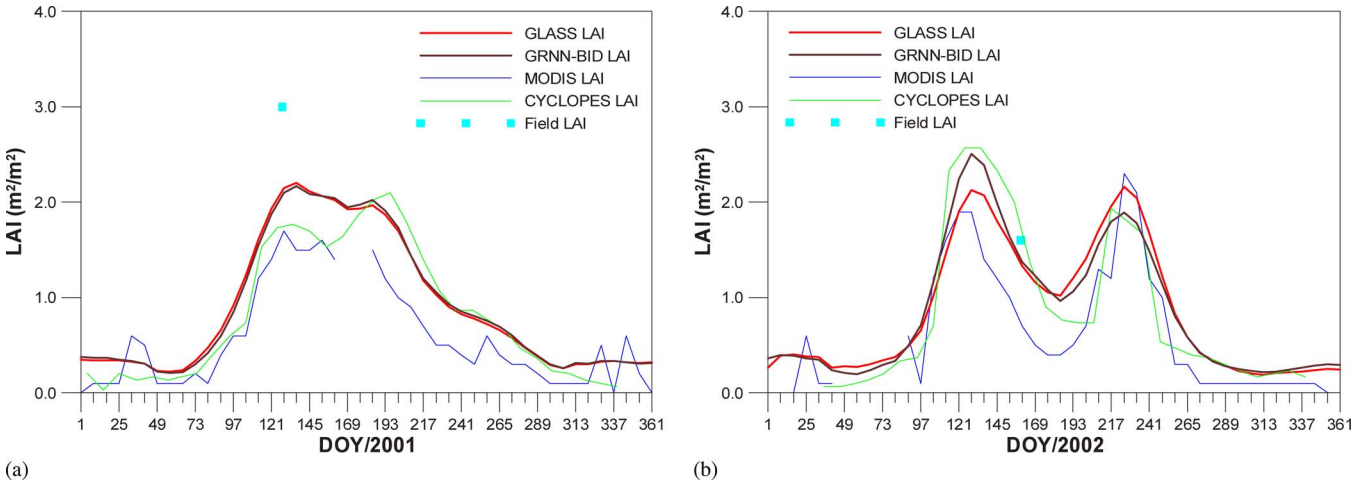

Fig. 11. Temporal profiles of GLASS, GRNN-BID, CYCLOPES, and MODIS LAI values for the Fundulea site for the years (a) 2001 and (b) 2002.

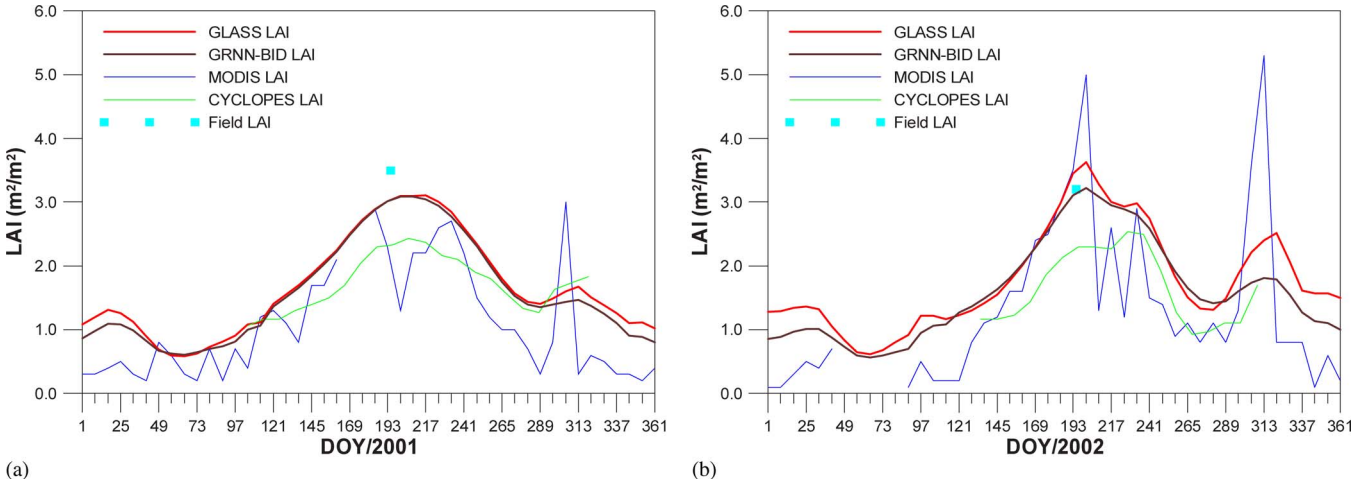

Fig. 12. Temporal profiles of GLASS, GRNN-BID, CYCLOPES, and MODIS LAI values at the NOBS-BOREAS site for the years (a) 2001 and (b) 2002.

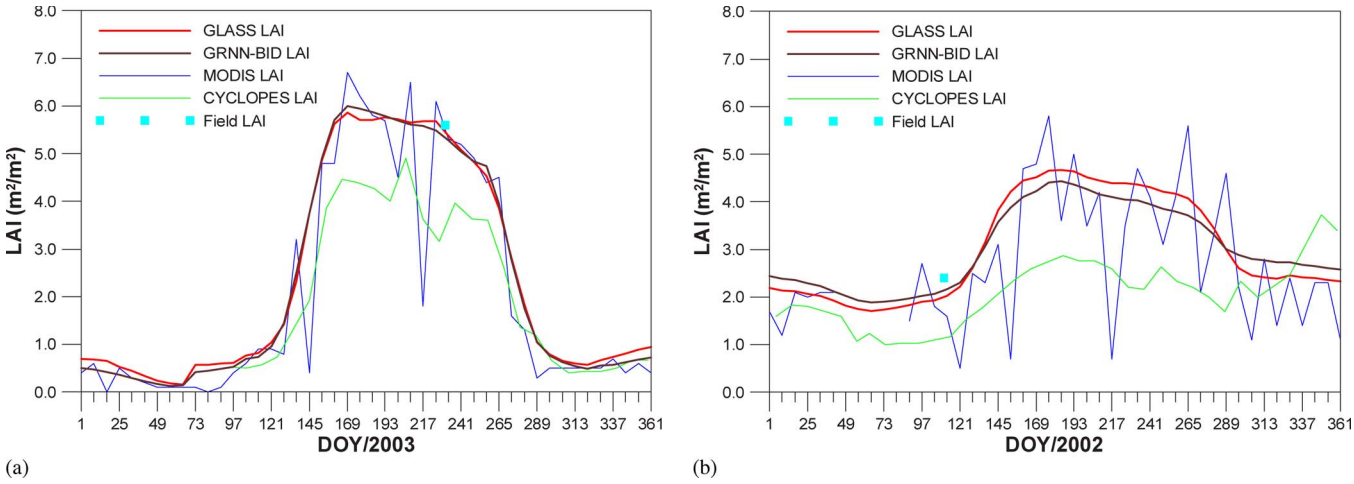

Fig. 13. Temporal profiles of GLASS, GRNN-BID, CYCLOPES, and MODIS LAI values at (a) the Larose site in 2003 and (b) the Nezer site in 2002.

underestimates throughout the entire growing season. The GLASS and GRNN-BID LAI values are in very good agreement with the BELMANIP mean LAI data at both sites.

Regarding broadleaf forests, the LAI temporal profiles at the Puechabon and Counami sites are illustrated in Fig. 14. The Puechabon site is largely dominated by trees of the species Quercus ilex, and it is classified as an evergreen broadleaf forest according to MODIS land cover. Large discrepancies are observed in the LAI magnitude between products at this site for the year 2001 [Fig. 14(a)]. The CYCLOPES LAI values exhibit an almost flat profile throughout the entire year. The GLASS, GRNN-BID, and MODIS LAI values exhibit similar temporal trajectories but with substantial differences in magnitude. The MODIS LAI values, except for dramatic fluctuations, are much

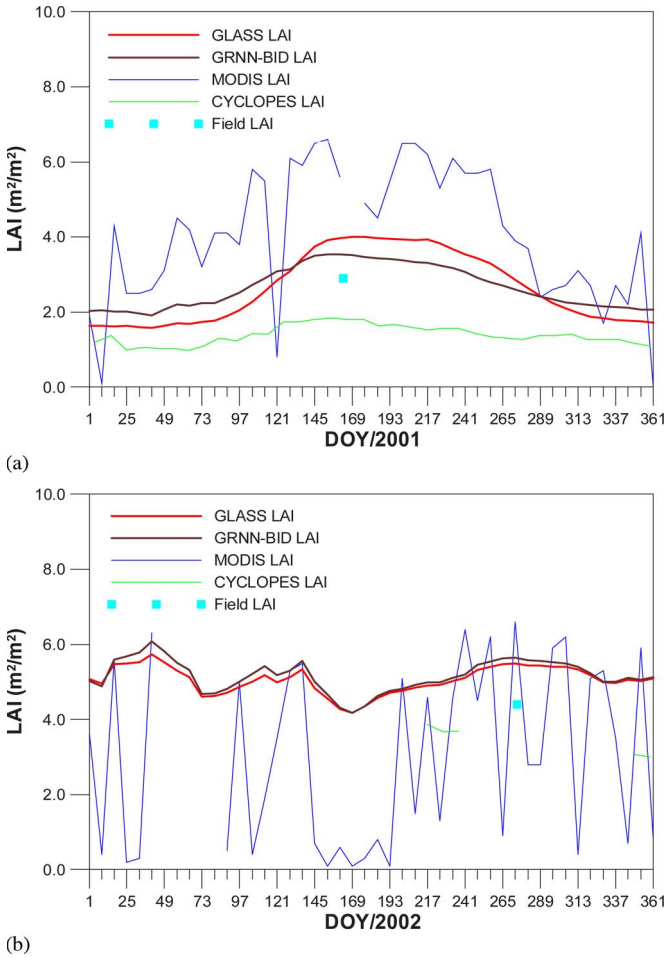

Fig. 14. Temporal profiles of GLASS, GRNN-BID, CYCLOPES, and MODIS LAI values at (a) the Puechabon site for the year 2001 and (b) the Counami site for the year 2002.

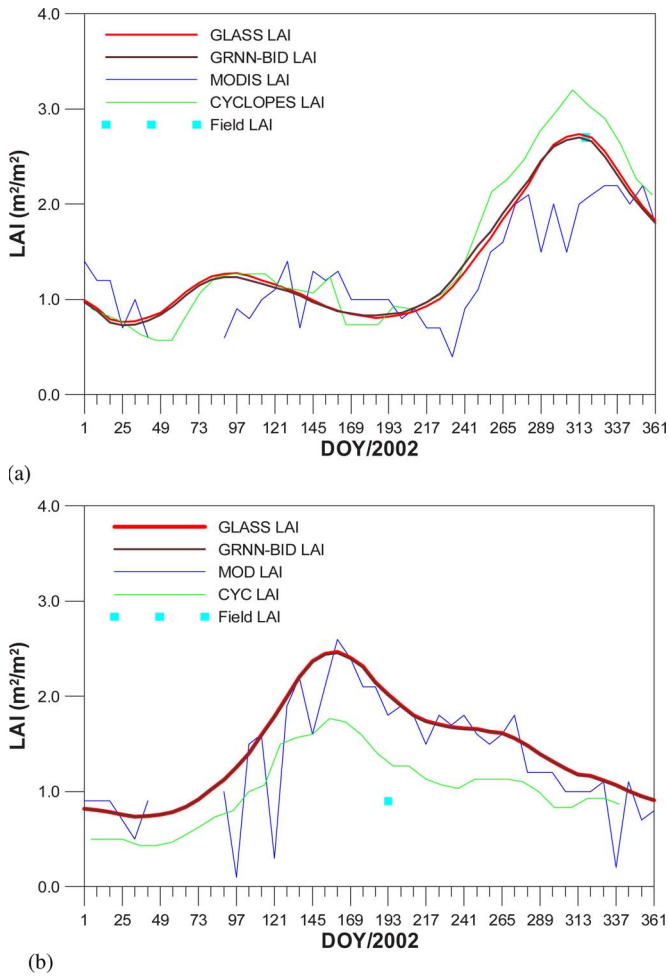

Fig. 15. Temporal profiles of GLASS, GRNN-BID, CYCLOPES, and MODIS LAI values at (a) the Laprida site for the year 2002 and (b) the Larzac site for the year 2002.

larger than either the GLASS and GRNN-BID LAI values or the mean BELMANIP LAI values. However, the GLASS and GRNN-BID LAI values are smooth, and the GLASS and GRNN-BID LAI values outperform the other LAI products in terms of accuracy when compared to the mean BELMANIP LAI data at this site. At the Counami site, visual inspection of the temporal profiles confirmed that the MODIS product is extremely shaky, and most of the CYCLOPES LAI estimates are missing; in fact, there are only five CYCLOPES LAI values for the entire year. Meanwhile, the GLASS and GRNN-BID LAI values are relatively smooth and close to the mean BELMANIP LAI values.

The temporal profiles of the GLASS, GRNN-BID, MODIS, and CYCLOPES LAI values at the Laprida and Larzac sites, which are of the savannah biome type, are provided in Fig. 15. At the Laprida site, the LAI temporal profiles were generally in very good agreement at the beginning of the growing season [Fig. 15(a)]. However, during the peak of the growing season, the MODIS LAI values became underestimates, and the CYCLOPES LAI values became overestimates in comparison with the mean BELMANIP LAI data at this site, while excellent agreement was achieved between the GLASS and GRNN-BID LAI values and the ground measurements. At the Larzac site [Fig. 15(b)], the GLASS, GRNN-BID, MODIS, and CYCLOPES LAI values showed similar temporal trajectories, although with differences in magnitude. The strongest agreement was achieved between the GLASS, GRNN-BID, and MODIS LAI values, although the MODIS LAI profile showed dramatic fluctuations; CYCLOPES maintained lower LAI values throughout the year. Fig. 15(b) also shows that the GLASS, GRNN-BID, MODIS, and CYCLOPES LAI values were all overestimates when compared to the ground-based LAI values.

V. Conclusion

A method of retrieving LAI values from time-series remote sensing data using a GRNN was developed in this study. The GRNN was trained using the fused LAI values calculated from MODIS and CYCLOPES LAI products and the corresponding reprocessed MODIS reflectance values. The input to the GRNN was the time-series reprocessed MODIS reflectance, and the output of the GRNN was the LAI profile for 1 year. A GRNN was constructed for each biome type according to the training database extracted from each BELMANIP site. Samples with different biome types were also used to train a biome-independent GRNN.

This study demonstrates that both the biome-dependent and biome-independent GRNNs are able to estimate temporally continuous LAI profiles, and the histograms of the GLASS and GRNN-BID LAI values show that the two distributions are

consistent between biomes. However, the GLASS LAI values agree somewhat better with the ground measurements than the GRNN-BID LAI values.

The GLASS and GRNN-BID LAI values were compared to the CYCLOPES and MODIS LAI products and were also validated by ground LAI measurements. The GLASS and GRNN-BID LAI values followed distributions consistent with those of the CYCLOPES and MODIS LAI values for the biome types of crops, grasses, shrubs, savannas, and needle forests. For the biome type of evergreen broadleaf forest, however, the GLASS and GRNN-BID LAI values were systematically higher than the CYCLOPES LAI values because the CYCLOPES algorithm does not include clumping at the plant and canopy scales, while the peak position of the MODIS LAI frequency distribution was higher compared to those of the GLASS and GRNN-BID LAI values due to the overestimation of the MODIS LAI values for broadleaf forests. At the selected BELMANIP sites, direct comparison with ground measurements shows that the accuracy of the GLASS and GRNN-BID LAI values is superior to the accuracy of the MODIS and CYCLOPES LAI values.

The retrieval method is being implemented to generate a long time series of global LAI products from MODIS and AVHRR data. It can also be applied to satellite data from other moderate-resolution sensors (e.g. VEGETATION) or similar sensors in the future. Theoretically, the method can be applied to the high-resolution sensors with the short revisit time (e.g., SENTINEL2), but how to get high-resolution time-series LAI with good quality to generate the training database must be addressed. Therefore, further considerations of the retrieval of LAI from time-series multi-sensor remote sensing data will be explored in a forthcoming study.

ACKNOWLEDGMENT

We would like to thank Dr. H. Tang and Mr. K Yu for re-processing MODIS surface reflectance data, Dr. X. Zhao for leading the team to generate the GLASS LAI product, and those who contributed to GLASS LAI production. We would also like to thank the CEOS LPV group for providing ground validation data on their website (http://lpvs.gsfc.nasa.gov/LPV_LAI10km.html).

REFERENCES

[1] J. Chen and T. A. Black, "Defining leaf area index for non-flat leaves," *Plant, Cell Environ.*, vol. 15, no. 4, pp. 421–429, May 1992.

[2] J. Chen, "Optically-based methods for measuring seasonal variation in leaf area index of boreal conifer forests," *Agric. Forest Meteorol.*, vol. 80, no. 2–4, pp. 135–163, Jul. 1996.

[3] S. Liang, *Quantitative Remote Sensing of Land Surfaces*. New York: Wiley, 2004.

[4] P. J. Sellers, S. O. Los, C. J. Tucker, C. O. Justice, D. A. Dazlich, G. J. Collatz, and D. A. Randall, "A revised land surface parameterization (SiB2) for atmospheric GCMS: Part II. The generation of global fields of terrestrial biophysical parameters from satellite data," *J. Climate*, vol. 9, no. 4, pp. 706–737, Apr. 1996.

[5] R. B. Myneni, R. R. Nemani, and S. W. Running, "Estimation of global leaf area index and absorbed PAR using radiative transfer model," *IEEE Trans. Geosci. Remote Sens.*, vol. 35, no. 6, pp. 1380–1393, Nov. 1997.

[6] J. Chen, G. Pavlic, L. Brown, J. Cihlar, S. G. Leblanc, H. P. White, R. J. Hall, D. Peddle, D. J. King, J. A. Trofymow, E. Swift, J. Van der Sanden, and P. Pellikka, "Derivation and validation of Canada-wide coarse-resolution leaf area index maps using ground measurements and high and moderate resolution satellite imagery," *Remote Sens. Environ.*, vol. 80, no. 1, pp. 165–184, Apr. 2002.

[7] C. Bacour, F. Baret, D. Béal, M. Weiss, and K. Pavageau, "Neural network estimation of LAI, fAPAR, fCover and LAI ×Cab, from top of canopy MERIS reflectance data: Principles and validation," *Remote Sens. Environ.*, vol. 105, no. 4, pp. 313–325, Dec. 2006.

[8] Z. Xiao, S. Liang, J. Wang, J. Song, and X. Wu, "A temporally integrated inversion method for estimating leaf area index from MODIS data," *IEEE Trans. Geosci. Remote Sens.*, vol. 47, no. 8, pp. 2536–2545, Aug. 2009.

[9] J. Qin, S. Liang, X. Li, and J. Wang, "Development of the adjoint model of a canopy radiative transfer model for sensitivity study and inversion of leaf area index," *IEEE Trans. Geosci. Remote Sens.*, vol. 46, no. 7, pp. 2028–2037, Jul. 2008.

[10] D. S. Kimes, Y. Knyazikhin, J. L. Privette, A. A. Abuelgasim, and F. Gao, "Inversion methods for physically-based models," *Remote Sens. Rev.*, vol. 18, no. 2–4, pp. 381–439, 2000.

[11] R. B. Myneni, S. Hoffman, Y. Knyazikhin, J. L. Privette, J. Glassy, Y. Tian, Y. Wang, X. Song, Y. Zhang, G. R. Smith, A. Lotsch, M. Friedl, J. T. Morisette, P. Votava, R. R. Nemani, and S. W. Running, "Global products of vegetation leaf area and absorbed PAR from year one of MODIS data," *Remote Sens. Environ.*, vol. 83, no. 1/2, pp. 214–231, Nov. 2002.

[12] G. Yang, C. Zhao, Q. Liu, W. Huang, and J. Wang, "Inversion of a radiative transfer model for estimating forest LAI from multisource and multiangular optical remote sensing data," *IEEE Trans. Geosci. Remote Sens.*, vol. 49, no. 3, pp. 988–1000, Mar. 2011.

[13] H. Fang and S. Liang, "Retrieving leaf area index with a neural network method: Simulation and validation," *IEEE Trans. Geosci. Remote Sens.*, vol. 41, no. 9, pp. 2052–2062, Sep. 2003.

[14] F. Baret, O. Hagolle, B. Geiger, P. Bicheron, B. Miras, M. Huc, B. Berthelot, F. Nino, M. Weiss, O. Samain, J. L. Roujean, and M. Leroy, "LAI, fAPAR and fCover CYCLOPES global products derived from VEGETATION. Part 1: Principles of the algorithm," *Remote Sens. Environ.*, vol. 110, no. 3, pp. 275–286, Oct. 2007.

[15] A. Verger, F. Baret, and M. Weiss, "Performances of neural networks for deriving LAI estimates from existing CYCLOPES and MODIS products," *Remote Sens. Environ.*, vol. 112, no. 6, pp. 2789–2803, Jun. 2008.

[16] H. Fang, S. Liang, J. Townshend, and R. Dickinson, "Spatially and temporally continuous LAI data sets based on an integrated filtering method: Examples from North America," *Remote Sens. Environ.*, vol. 112, no. 1, pp. 75–93, Jan. 2008.

[17] L. E. O. C. Aragao, Y. E. Shimabukuro, F. D. B. Espirito-Santo, and M. Williams, "Spatial validation of the collection 4 MODIS LAI product in eastern Amazonia," *IEEE Trans. Geosci. Remote Sens.*, vol. 43, no. 11, pp. 2526–2534, Nov. 2005.

[18] P. Yang, R. Shibasaki, W. Wu, Q. Zhou, Z. Chen, Y. Zha, Y. Shi, and H. Tang, "Evaluation of MODIS land cover and LAI products in cropland of North China plain using in situ measurements and Landsat TM images," *IEEE Trans. Geosci. Remote Sens.*, vol. 45, no. 10, pp. 3087–3097, Oct. 2007.

[19] Z. Xiao, J. Wang, S. Liang, Y. Qu, and H. Wan, "Retrieval of canopy biophysical variables from remote sensing data using contextual information," *J. Central South Univ. Technol.*, vol. 15, no. 6, pp. 877–881, Dec. 2008.

[20] Q. Liu, L. Gu, R. E. Dickinson, Y. Tian, L. Zhou, and W. M. Post, "Assimilation of satellite reflectance data into a dynamical leaf model to infer seasonally varying leaf areas for climate and carbon models," *J. Geophys. Res.*, vol. 113, no. D19, p. D19 113, Oct. 2008.

[21] Z. Xiao, S. Liang, J. Wang, B. Jiang, and X. Li, "Real-time retrieval of leaf area index from MODIS time series data," *Remote Sens. Environ.*, vol. 115, no. 1, pp. 97–106, Jan. 2011.

[22] Y. Knyazikhin, J. V. Martonchik, R. B. Myneni, D. J. Diner, and S. W. Running, "Synergistic algorithm for estimating vegetation canopy leaf area index and fraction of absorbed photosynthetically active radiation from MODIS and MISR data," *J. Geophys. Res.*, vol. 103, no. D24, pp. 32 257–32 275, Jan. 1998.

[23] G. Zhu, W. Ju, J. Chen, P. Gong, B. Xing, and J. Zhu, "Foliage clumping index over China's landmass retrieved from the MODIS BRDF parameters product," *IEEE Trans. Geosci. Remote Sens.*, vol. 50, no. 6, pp. 2122–2137, Jun. 2012.

[24] S. Garrigues, R. Lacaze, F. Baret, J. T. Morisette, M. Weiss, J. E. Nickeson, R. Fernandes, S. Plummer, N. V. Shabanov, R. B. Myneni, Y. Knyazikhin, and W. Yang, "Validation and intercomparison of global Leaf Area Index products derived from remote sensing data," *J. Geophys. Res.*, vol. 113, no. G2, p. G02 028, Jun. 2008.

[25] D. Huang, Y. Knyazikhin, R. E. Dickinson, M. Rautiainen, P. Stenberg, M. Disney, P. Lewis, A. Cescatti, Y. Tian, W. Verhoef, J. V. Martonchik, and R. B. Myneni, "Canopy spectral invariants for remote sensing and model applications," *Remote Sens. Environ.*, vol. 106, no. 1, pp. 106–122, Jan. 2007.

[26] M. A. Friedl, D. K. McIver, J. C. F. Hodges, X. Y. Zhang, D. Muchoney, A. H. Strahler, C. E. Woodcock, S. Gopal, A. Schneider, and A. Cooper, "Global land cover mapping from MODIS: Algorithms and early results," *Remote Sens. Environ.*, vol. 83, no. 1/2, pp. 287–302, Nov. 2002.
[27] *GCTP General Cartographic Transformation Package Software Documentation*, U.S. Geological Survey, National Mapping Division, Reston, VA, 1993.
[28] C. Justice, A. Belward, J. Morisette, P. Lewis, J. Privette, and F. Baret, "Developments in the "validation" of satellite sensor products for the study of the land surface," *Int. J. Remote Sens.*, vol. 21, no. 17, pp. 3383–3390, 2000.
[29] J. Wang and X. Li, "Knowledge database and inversion," in *Advances in Land Remote Sensing: System, Modeling, Inversion and Application*, S. Liang, Ed. New York: Springer-Verlag, 2008, ch. 8, pp. 203–217.
[30] A. R. G. Lang and Y. Xiang, "Estimation of leaf area index from transmission of direct sunlight in discontinuous canopies," *Agric. Forest Meteorol.*, vol. 37, no. 3, pp. 229–243, Aug. 1986.
[31] J. Chen, C. Menges, and S. Leblanc, "Global mapping of foliage clumping index using multi-angular satellite data," *Remote Sens. Environ.*, vol. 97, no. 4, pp. 447–457, Sep. 2005.
[32] J. Pisek, J. Chen, R. Lacaze, O. Sonnentag, and K. Alikas, "Expanding global mapping of the foliage clumping index with multi-angular POLDER three measurements: Evaluation and topographic compensation," *ISPRS J. Photogramm. Remote Sens.*, vol. 65, no. 4, pp. 341–346, Jul. 2010.
[33] D. Wang and S. Liang, "Integrating MODIS and CYCLOPES leaf area index products using empirical orthogonal functions," *IEEE Trans. Geosci. Remote Sens.*, vol. 49, no. 5, pp. 1513–1519, May 2011.
[34] J. M. Chen, F. Deng, and M. Z. Chen, "Locally adjusted cubic-spline capping for reconstructing seasonal trajectories of a satellite-derived surface parameter," *IEEE Trans. Geosci. Remote Sens.*, vol. 44, no. 8, pp. 2230–2238, Aug. 2006.
[35] H. Tang, K. Yu, X. Geng, Y. Zhao, K. Jiang, and S. Liang, "A time series method for cloud detection applied to MODIS surface reflectance images," *Int. J. Digit. Earth*, 2013, to be published.
[36] D. F. Specht, "A general regression neural network," *IEEE Trans. Neural Netw.*, vol. 2, no. 6, pp. 568–576, Nov. 1991.
[37] M. T. Leung, A. S. Chen, and H. Daouk, "Forecasting exchange rates using general regression neural networks," *Comput. Oper. Res.*, vol. 27, no. 11/12, pp. 1093–1110, Sep. 2000.
[38] F. Baret, J. T. Morisette, R. A. Fernandes, J. L. Champeaux, R. B. Myneni, J. Chen, S. Plummer, M. Weiss, C. Bacour, S. Garrigues, and J. Nickeson, "Evaluation of the representativeness of networks of sites for the global validation and intercomparison of land biophysical products: Proposition of the CEOS-BELMANIP," *IEEE Trans. Geosci. Remote Sens.*, vol. 44, no. 7, pp. 1794–1803, Jul. 2006.
[39] J. Hansen and R. Meservy, "Learning experiments with genetic optimization of a generalized regression and neural network," *Decision Support Syst.*, vol. 18, no. 3/4, pp. 317–325, Nov. 1996.
[40] Q. Duan, S. Sorooshian, and V. K. Gupta, "Effective and efficient global optimization for conceptual rainfall-runoff models," *Water Resour. Res.*, vol. 28, no. 4, pp. 1015–1031, 1992.
[41] Z. Xiao, J. Wang, S. Liang, H. Zhou, X. Li, L. Zhang, Z. Jiao, Y. Liu, and Z. Fu, "Variational retrieval of leaf area index from MODIS time series data: Examples from the Heihe River Basin, North-west China," *Int. J. Remote Sens.*, vol. 33, no. 3, pp. 730–745, Feb. 2012.
[42] S. Liang, H. Fang, M. Z. Chen, C. J. Shuey, C. Walthall, C. Daughtry, J. Morisette, C. Schaaf, and A. Strahler, "Validating MODIS land surface reflectance and albedo products: Methods and preliminary results," *Remote Sens. Environ.*, vol. 83, no. 1/2, pp. 149–162, Nov. 2002.
[43] N. V. Shabanov, D. Huang, W. Yang, B. Tan, Y. Knyazikhin, R. B. Myneni, D. E. Ahl, S. T. Gower, A. R. Huete, L. E. Aragão, and Y. E. Shimabukuro, "Analysis and optimization of the MODIS Leaf Area Index algorithm retrievals over broadleaf forests," *IEEE Trans. Geosci. Remote Sens.*, vol. 43, no. 8, pp. 1855–1865, Aug. 2005.

Zhiqiang Xiao received the Ph.D. degree in geophysical prospecting and information technology from Central South University, Changsha, China, in 2004.

From 2004 to 2006, he was a Postdoctoral Research Associate with Beijing Normal University, Beijing, China. His research focuses on retrieval of land biophysical parameters from remotely sensed data, assimilating radiometric observations into dynamic models.

Shunlin Liang (M'94–SM'01) received the Ph.D. degree in remote sensing and geographic information system from Boston University, Boston, MA.

He was a Postdoctoral Research Associate with Boston University from 1992 to 1993 and a Validation Scientist with the NOAA/NASA Pathfinder AVHRR Land Project from 1993 to 1994. He is currently a Professor with the University of Maryland, College Park. His main research interests focus on spatio-temporal analysis of remotely sensed data, integration of data from different sources and numerical models, and linkage of remote sensing with carbon and water cycles. He authored the book Quantitative Remote Sensing of Land Surfaces (Wiley, 2004) and edited the book Advances in Land Remote Sensing: System, Modeling, Inversion, and Application (Springer, 2008).

Dr. Liang is a member of NASA ASTER and MODIS science teams and a Co-chairman of the International Society for Photogrammetry and Remote Sensing Commission VII/I Working Group on Fundamental Physics and Modeling. He is an Associate Editor of the IEEE TRANSACTIONS ON GEOSCIENCE AND REMOTE SESING.

Jindi Wang graduated from the Beijing University of Posts and Telecommunications, Beijing, China, in 1982.

Currently, she is a Professor at the State Key Laboratory of Remote Sensing Science, Research Center for Remote Sensing and Geographic Information Systems, Beijing Normal University, Beijing, China. Her primary research interests focus on land surface bidirectional reflectance distribution function modeling, land surface parameters retrieval, typical land surface objects' spectrum library building, and its application.

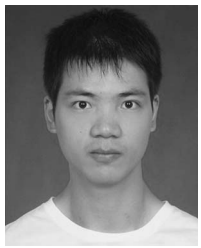

Ping Chen received the B.S. degree in geography information systems from the Nanjing University, Nanjing, China, in 2007, and received the M.S. degree in remote sensing and geographic information system from Beijing Normal University, Beijing, China, in 2012.

His current research is focused on retrieval of land surface parameters from remote sensing data and on land surface data assimilation.

Xuejun Yin received the B.S. degree in geography information systems from the Nanjing Normal University, Nanjing, China, in 2009, and received the M.S. degree in remote sensing and geographic information system from Beijing Normal University, Beijing, China, in 2012.

Her current research is focused on retrieval of biophysical variables from remote sensing data.

Liqiang Zhang received the Ph.D. degree in geoinformatics from the Chinese Academy of Science's Institute of Remote Sensing Applications, Beijing, China, in 2004. Currently, he is a Professor at the School of Geography, Beijing Normal University, Beijing, China.

His research interests include remote sensing image processing, 3-D urban reconstruction, and spatial object recognition.

Jinling Song received the Ph.D. degree in remote sensing and geographic information system from Beijing Normal University, Beijing, China, in 2006.

She was a Postdoctoral Research Associate with Beijing Normal University from 2006 to 2008. Her research is directed toward computer simulation and parameter retrieval of vegetation.